ADVANCED FUNCTIONAL MATERIALS

Anisotropy and Dynamic Ranges in Effective Properties of Sheared Nematic Polymer Nanocomposites**

By *M. Gregory Forest*,* *Xiaoyu Zheng*, *Ruhai Zhou*, *Qi Wang*, and *Robert Lipton*

Nematic, or liquid-crystalline, polymer nanocomposites (NPNCs) are composed of large aspect ratio, rod-like or platelet, rigid macromolecules in a matrix or solvent, which itself may be aqueous or polymeric. NPNCs are engineered for high-performance material applications, ranging across mechanical, electrical, piezoelectric, thermal, and barrier properties. The rods or platelets possess enormous property contrasts relative to the solvent, yet the composite properties are strongly affected by the orientational distribution of the nanophase. Nematic polymer film processing flows are shear-dominated, for which orientational distributions are well known to be highly sensitive to shear rate and volume fraction of the nematogens, with unsteady response being the most expected outcome at typical low shear rates and volume fractions. The focus of this article is a determination of the ranges of anisotropy and dynamic fluctuations in effective properties arising from orientational probability distribution functions generated by steady shear of NPNC monodomains. We combine numerical databases for sheared monodomain distributions[1,2] of thin rod or platelet dispersions together with homogenization theory for low-volume-fraction spheroidal inclusions[3] to calculate effective conductivity tensors of steady and oscillatory sheared mesophases. We then extract maximum scalar conductivity enhancement and anisotropy for each type of sheared monodomain (flow-aligned, tumbling, kayaking, and chaotic).

1. Introduction

There is rich recent literature on the remarkable shear-induced responses of nematic (liquid-crystalline) polymers (LCPs) in a viscous solvent. We refer the reader to recent articles[1,2,4–11] where dynamical systems bifurcation tools and continuation software (AUTO) have led to a nearly complete understanding of shear-imposed bulk behavior of NPNCs. A full coupling, with hydrodynamic feedback and spatial gradients in the orientational distribution, is orders of magnitude more difficult, and our understanding remains primitive.[1,2,12–21] Textured LCP composites may be viewed as a spatial distribution of monodomains, where locally the monodomains may be steady or unsteady during processing. The results of this paper apply to these local sheared monodomains, whose quantitative features will be modified through spatial coupling and distortional elasticity. Indeed, in a previous publication,[21] we combined results from the present paper, Zhou et al.,[15] and Zheng et al.[3] to indicate heterogeneous effective properties. Another important effect in NPNCs is strong density variations of the nano-elements; there are no modeling results thus far on flow processing with density fluctuations, to our knowledge.

The advances in this paper are based on an implementation of the connection developed in Zheng et al.[3] between the probability distribution function (PDF, $f(\boldsymbol{m},t)$, where $\boldsymbol{m}$ is the molecular orientation and t is time) of sheared nematic polymer monodomains and the effective electrical conductivity tensor, $\boldsymbol{\Sigma}^e$, of low-volume-fraction nanocomposite materials. Here we extend our previous results from steady to transient bulk phases, and we use resolved kinetic-theory databases for the orientation distribution functions of the nanorods in replacing the approximate second-moment models. We use numerical monodomain attractors of the Doi–Hess kinetic theory, sampling at shear rates and nematic polymer concentrations associated with the various steady and oscillatory responses.

For each sheared monodomain, we extract the maximum principle value, σ_{max}, of the effective conductivity tensor, $\boldsymbol{\Sigma}^e$, whose value relative to the isotropic conductivity, σ_1, of the matrix solvent depicts the maximum scalar enhancement,

[*] Prof. M. G. Forest, X. Zheng
Department of Mathematics, Institute for Advanced Materials, Nanoscience, and Technology
University of North Carolina at Chapel Hill
Chapel Hill, NC 27599 (USA)
E-mail: forest@amath.unc.edu
Dr. R. Zhou
Department of Mathematics and Statistics
Old Dominion University
Norfolk, VA 23529 (USA)
Prof. Q. Wang
Department of Mathematical Sciences
Florida State University
Tallahassee, FL 32306 (USA)
Prof. R. Lipton
Department of Mathematics
Louisiana State University
Baton Rouge, LA 70803 (USA)

[**] Effort sponsored by the Air Force Office of Scientific Research, F49620–02–6–0086, F49620–03–1–0098, FA9550–05–1–0008, Air Force Materials Command, USAF, the National Science Foundation through grants DMS-0204243, DMS-0308019, DMS-0406374, and the Army Research Office, under grant number W911 NF-04-D-0004. This work is supported in part by the NASA University Research, Engineering and Technology Institute on Bio Inspired Materials (BIMat) under award No. NCC-1–02037.

 DOI: 10.1002/adfm.200500272

$\varepsilon_{\max} = (\sigma^e_{\max} - \sigma_1)/\sigma_1$, due to the nematic polymer inclusions. To convey anisotropy in effective conductivity, we also give the difference $(\sigma^e_1 - \sigma^e_2)$ in the leading two principal values, $\sigma^e_1 \geq \sigma^e_2 \geq \sigma^e_3$, of $\boldsymbol{\Sigma}^e$. In all figures, conductivities are normalized and shown as enhancements, $\varepsilon_j = (\sigma^e_j - \sigma_1)/\sigma_1$, where $j = 1, 2, 3$. In this measure, the order of magnitude of ε_j compared with that of the nanophase/matrix contrast, σ_2/σ_1, conveys the essential nanocomposite property information.

For steady monodomains, the conductivity tensor is constant, for which we exhibit parametric variations in $\varepsilon_{\max}$ versus shear rate and nanorod volume fraction. For oscillatory monodomains, we consider representative tumbling, kayaking, and chaotic attractors and show the corresponding dynamic ranges of $\varepsilon_{\max}$ and $\varepsilon_1 - \varepsilon_2$, and the principal axes, $\boldsymbol{n}_i$, of $\boldsymbol{\Sigma}^e$ (associated with principal values, σ^e_i) are identical with the three major axes of the second-moment of the PDF, $\boldsymbol{M}(f)$. These orthogonal directions are known in the liquid-crystal and nematic-polymer literature as the directors of the PDF. The maximum scalar conductivity, $\sigma^e_1 = \sigma^e_{\max}$, of the NPNC is associated with $\boldsymbol{n}_1$, the major director of the PDF, i.e., the peak axis of the orientational distribution function. These connections are established by Zheng et al.[3]

The outline of the paper is the following: we recall key elements of the kinetic theory of Doi and Hess for sheared nematic polymers in a viscous solvent, and of the effective-conductivity tensor for high-aspect-ratio spheroidal ensembles at low volume fractions. We then implement these results for representative steady and unsteady distribution functions.

2. Kinetic Theory for Sheared Nematic Polymers

Let $f(\boldsymbol{m},t)$ be the orientational PDF for rod-like, rigid, extremely high aspect ratio molecules with an axis of symmetry, $\boldsymbol{m}$, on the unit sphere, S^2. The Smoluchowski equation for $f(\boldsymbol{m},t)$ in a flow field, $\boldsymbol{v}$, is given by:[22,23]

$$\begin{aligned} \frac{\mathrm{D}f}{\mathrm{D}t} &= \Re[D_r(\boldsymbol{m})(\Re f + \frac{1}{kT} f \Re V)] - \Re \cdot [\boldsymbol{m} \times \dot{\boldsymbol{m}} f], \\ \dot{\boldsymbol{m}} &= \boldsymbol{\Omega} \cdot \boldsymbol{m} + a[\boldsymbol{D} \cdot \boldsymbol{m} - \boldsymbol{D} : \boldsymbol{mmm}], \end{aligned} \tag{1}$$

where $D_r(\boldsymbol{m})$ is the rotary diffusivity which we hold constant, $D_r(\boldsymbol{m}) = D^0_r$, consistent with the work of Forest et al.,[1] Faraoni et al.,[8] and Grosso et al.;[24] k is the Boltzmann constant; T is absolute temperature; $\Re = \boldsymbol{m} \times \partial/\partial \boldsymbol{m}$ is the rotational gradient operator; $\mathrm{D}/\mathrm{D}t\,(\cdot)$ denotes the material derivative $\partial/\partial t\,(\cdot) + \boldsymbol{v} \cdot \nabla(\cdot)$; V is the excluded-volume potential; and $\boldsymbol{\Omega}$ is the vorticity tensor. The geometry parameter, a, is related to the aspect ratio, r, of the spheroidal molecule by

$$a = \frac{r^2 - 1}{r^2 + 1}. \tag{2}$$

We consider simple shear flow in Cartesian coordinates (x, y, z) with shear rate, $\dot{\gamma}$, x is the flow direction, y is the flow-gradient direction, and z is the vorticity axis,

$$\boldsymbol{v} = \dot{\gamma}(y, 0, 0). \tag{3}$$

$\boldsymbol{D}$ and $\boldsymbol{\Omega}$ in Equation 1 are the corresponding rate-of-strain and vorticity tensors,

$$\boldsymbol{D} = \frac{1}{2}\dot{\gamma}\begin{pmatrix} 0 & 1 & 0 \\ 1 & 0 & 0 \\ 0 & 0 & 0 \end{pmatrix}, \boldsymbol{\Omega} = \frac{1}{2}\dot{\gamma}\begin{pmatrix} 0 & 1 & 0 \\ -1 & 0 & 0 \\ 0 & 0 & 0 \end{pmatrix}. \tag{4}$$

The Peclet number, Pe ($Pe = \dot{\gamma}/D^0_r$, where the shear rate, $\dot{\gamma}$, is imposed by controlled plate speeds relative to the thickness of the film, and D_r is the mean rotational diffusion constant of the nematic liquid), is the normalized flow-rate parameter. The second-moment of the PDF,

$$\boldsymbol{M} = \langle \boldsymbol{mm} \rangle = \int_{\|\boldsymbol{m}\|=1} \boldsymbol{mm} f(\boldsymbol{m}, t)\, \mathrm{d}\boldsymbol{m}, \tag{5}$$

determines the mean-field, Maier–Saupe excluded-volume potential,

$$V = -\frac{3}{2} N kT\, \boldsymbol{mm} : \boldsymbol{M}, \tag{6}$$

where N is the dimensionless strength of the potential, V, proportional to the volume fraction, θ_2, of the nematic polymer inclusions by

$$\theta_2 = \frac{N\pi}{8r}, \tag{7}$$

where $r = l/d$ is the nematogen aspect ratio, l is the length, and d is the diameter. The mesoscopic orientation tensor, $\boldsymbol{Q}$, is the traceless part of $\boldsymbol{M}$,

$$\boldsymbol{Q} = \boldsymbol{M} - 1/3\, \boldsymbol{I}, \tag{8}$$

which provides the link between the PDF $f(\boldsymbol{m},t)$ and rheological measurements of principle directions and degrees of alignment, and of shear stress and normal stress differences. In a previous publication,[1,2] we provide phase diagrams of all stable solutions, $f(\boldsymbol{m},t)$, of this Doi–Hess model in the two-parameter space of (θ_2, Pe). These stable states are steady only at sufficiently low and high volume fractions, or at sufficiently high shear rates. The rest of the phase diagram is dominated by dynamic PDFs, including periodic limit cycles of various types and a finite region with chaotic response. We refer to these papers for details, and here we will pick representative PDFs with which we then calculate the effective conductivity tensor either in steady state or in real processing time on the attractors. We then compress these data into a representative "property bifurcation diagram", providing a property analog of now-standard PDF phase diagrams.

ADVANCED FUNCTIONAL MATERIALS

3. Effective Conductivity Tensors of NPNCs

Suppose spheroidal molecules with aspect ratio r, isotropic electrical conductivity σ_2, and volume fraction θ_2 are populated in an isotropic matrix of electrical conductivity σ_1 according to the orientational probability distribution function $f(\boldsymbol{m})$ of the ensemble. Then, the effective electrical conductivity tensor $\boldsymbol{\Sigma}^e$ can be expressed in the low-volume-fraction limit ($\theta \ll 1$) as[3] a linear function of $\boldsymbol{M}(f)$, the second moment of the PDF (Equation 5):

$$\boldsymbol{\Sigma}^e = \sigma_1 \left[\boldsymbol{I} + \frac{2\theta_2 \beta}{1+\beta(1-L_a)} \left(\boldsymbol{I} + \beta \frac{1-3L_a}{1+2\beta L_a} \boldsymbol{M} \right) \right], \tag{9}$$

where the factors L_a and β are explicit functions of molecule geometry (r) and conductivity contrast (σ_1/σ_2), respectively,

$$L_a = \frac{1}{(r^2-1)} \left(\frac{r}{\sqrt{r^2-1}} \ln(r+\sqrt{r^2-1}) - 1 \right), \tag{10}$$

$$\beta = \frac{\sigma_2 - \sigma_1}{2\sigma_1}. \tag{11}$$

The three principal axes of the effective conductivity are, by Equation 9, identical with the principal axes of the second moment tensor $\boldsymbol{M}(f)$. The three principle conductivity values (eigenvalues of $\boldsymbol{\Sigma}^e$) are denoted by $\sigma_1^e \geq \sigma_2^e \geq \sigma_3^e$; the largest value, σ_1, is the maximum effective conductivity. The relative principal value enhancements are given by

$$\varepsilon_i = \frac{(\boldsymbol{\Sigma}^e - \sigma_1 \boldsymbol{I})}{\sigma_1} : \boldsymbol{n}_i \boldsymbol{n}_i = \frac{\sigma_i^e - \sigma_1}{\sigma_1}, \qquad i = 1,2,3 \tag{12}$$

where $\boldsymbol{n}_i$ is the principle axis. Note that $\varepsilon = 0$ if there is no conductivity contrast, i.e., $\sigma_1^{nano} = \sigma_1^{matrix}$, and $\varepsilon = 1$ implies $\sigma_1^e = 2\sigma_1^{matrix}$ or 100 % gain of the bulk composite conductivity, which is to be compared with the order of magnitude of $2\beta = (\sigma_2 - \sigma_1)/\sigma_1$, the microscopic enhancement. More generally, $\varepsilon \sim O(10^k)$ implies k orders of magnitude gain. We order the enhancements, $\varepsilon_1 \geq \varepsilon_2 \geq \varepsilon_3$, so that ε_1 captures the major enhancement, whereas $\varepsilon_1 - \varepsilon_2$ measures property anisotropy with respect to the two principal conductivity directions, $\boldsymbol{n}_1$, $\boldsymbol{n}_2$.

4. Enhancement and Anisotropy in Effective Conductivity of Representative Sheared NPNC Monodomains

We consider typical model NPNCs with the nematogen aspect ratio $r = 200$ (and one with $r = 50$ for comparison). For $r = 200$, the prefactor, L_a, in Equations 9,10 is $O(10^{-4})$; for $r = 50$, L_a is 10^{-3}. We specify the conductivity contrast between the nanophase and the matrix solvent as $\sigma_2/\sigma_1 = 10^6$. These specifications obey the inequality $L_a \gg (\sigma_1/\sigma_2)$, in which case the scaling law in the publication by Zheng et al.[3] yields a simplified estimate for the effective conductivity tensor, (Equation 9):

$$\boldsymbol{\Sigma}^e \approx \sigma_1 (\boldsymbol{I} + \frac{\theta_2}{L_a} \boldsymbol{M}), \quad \varepsilon_j \approx \frac{\theta_2}{L_a} d_j, j = 1,2,3. \tag{13}$$

Recall that d_j represents the three eigenvalues of $\boldsymbol{M}$, $0 \leq d_j \leq 1$. We now appeal to the "monodomain phase diagram" of Doi–Hess kinetic theory, as developed by Forest et al.[1,2] In these papers, we give the shear-induced mesophase attractors for high-aspect-ratio rod nematogens. The phase diagram compiles the PDF $f(\boldsymbol{m},t)$ versus two fundamental control parameters. The key composition parameter is the volume fraction, θ_2, of the nematogen inclusions. The key processing parameter is the normalized steady shear rate, or the Peclet number.

The monodomain attractors consist of steady, so-called flow-aligned (FA) states, for which the PDF $f(\boldsymbol{m})$ is a steady solution of the kinetic Smoluchowski equation (Equations 1–6), and dynamic solutions $f(\boldsymbol{m},t)$, which are periodic limit cycles of various types, or chaotic attractors which arise from different period-doubling bifurcation sequences. The periodic sheared monodomains are called *tumbling* if the major director, $\boldsymbol{n}_1$, of $\boldsymbol{M}(f)$ rotates monotonically in the plane of shear (the flow–flow gradient plane), and *wagging* if $\boldsymbol{n}_1$ oscillates with finite amplitude in the shear plane. An FA state may have the peak of the PDF, $\boldsymbol{n}_1$, aligned in the shear plane at an angle called the Leslie alignment angle or normal to the shear plane along the vorticity axis, in which the attractor is called *logrolling*. (Other out-of-plane alignment possibilities exist, but they are experimentally unlikely.) In addition to the "in-plane" oscillatory responses, there are *kayaking* orbits, in which $\boldsymbol{n}_1$ rotates monotonically around the vorticity axis, and *tilted kayaking* orbits, in which $\boldsymbol{n}_1$ rotates around some out-of-plane direction between the vorticity axis and the shear plane. Finally, there are chaotic monodomain attractors, which have highly irregular dynamics, arising from period-doubling bifurcation routes to chaos.

We proceed now to sample from within regions in (θ, Pe), where each of these attracting sheared responses occur, and extract the important effective conductivity features from the analytical framework described in Section 3.

For FA states, Figure 1 shows the peak axis (Leslie alignment angle) of the steady PDF and maximum scalar conductivity enhancement (ε_{max}) versus Pe for three different volume fractions, θ_2. These correspond to slices of the region I in the publication of Forest et al.[2] at $N = 4.7$, 5.5, 6 ($\theta_2 = 0.92$, 1.08, 1.26 % for $r = 200$; $\theta_2 = 3.69$, 4.32, 5.03 % for r = 50; at rest, each nematic liquid is isotropic at lowest volume fraction and nematic at the other two). Note that as the volume fraction increases so does the shear rate required to induce steady alignment. The primary result from Figure 1b is the prediction that the maximum scalar conductivity, σ_{max}^e, of the NPNC monodomain is 50–75 times the isotropic matrix conductivity, σ_1. Thus, for these sheared

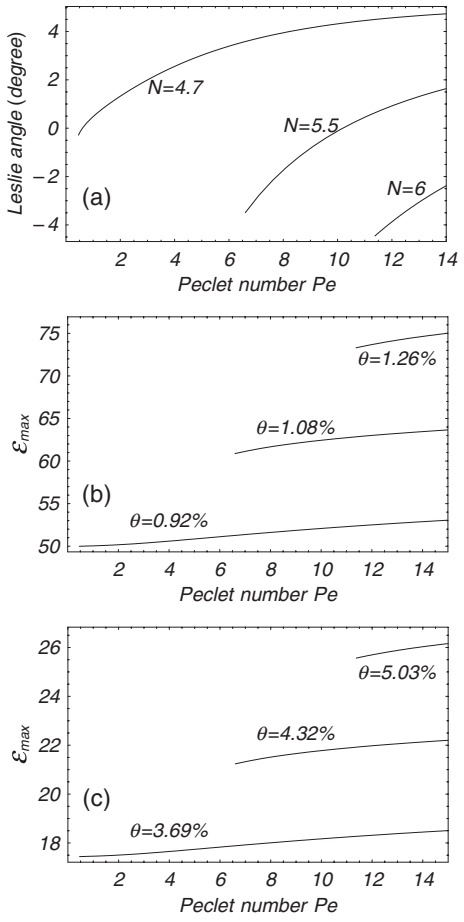

Figure 1. Peak alignment angle (a) and maximum scalar conductivity enhancement (b,c) for families of flow-aligned steady states. (a) shows normalized concentrations $N = 4.7$, 5.5,6. These values of N are equivalent to volume fractions of 0.92, 1.08, and 1.26 %, respectively, for a nanorod aspect ratio of 200, depicted in (b), and also equivalent to volume fractions 3.69, 4.32, and 5.03 %, respectively, for nanorods of aspect ratio 50 (c). These steady orientational states exist and are stable over the indicated ranges of normalized shear rate (Pe).

composites, one captures two orders of magnitude gain at these extremely low volume fractions from the upper limit of six orders of magnitude in property contrast: $\sigma_2/\sigma_1 = 10^6$.

The second result for these FA steady states from Figure 1 is that $\partial\varepsilon_{max}/\partial Pe \approx 0.2$ for $r = 200$, so that there is a considerable benefit to ε_{max} in shearing near the highest shear rate of stability of these FA states. If we lower the aspect ratio to $r = 50$, then $\partial\varepsilon_{max}/\partial Pe \approx 0.06$, so the enhancement due to increased shear rate is quite weak. At higher θ_2 or N, which require higher Pe to stabilize the FA phase, one finds an additional 20–50 % rise in ε_{max} for both aspect ratios. Comparing Figures 1b,c with different aspect ratios and the same normalized concentration, N, the lower aspect ratio corresponds to higher volume fraction and, consistent with the scaling law (Equation 13), the relative enhancement drops by 2/3. We can conclude that aspect ratio is a dominant factor in controlling the effective electrical conductivity. For the remaining simulations and figures, we restrict r to 200.

Figure 2 shows the major enhancement for steady logrolling (LR) states, for which the principal axis, $\boldsymbol{n}_1$, lies along the flow vorticity direction, and $\boldsymbol{n}_2$ lies in the flow–flow gradient plane. As volume fraction increases, the Pe window of stable LR states widens, in contrast to Figure 1 and FA states. We again give results for three concentrations versus shear rate. The maximum scalar conductivity, σ_{max}, of LR NPNC monodomain distribution functions is on the order of 68–78 times the matrix conductivity, σ_1. These enhancements are slightly greater (>10 %) than FA steady distributions at comparable volume fractions, and these PDFs are achievable at significantly lower shear rates. We note further from Figure 2, that $\partial\varepsilon_{max}/\partial Pe \approx -0.5$, so that it is advantageous to operate near the lowest stable shear rates for LR states at a given volume fraction.

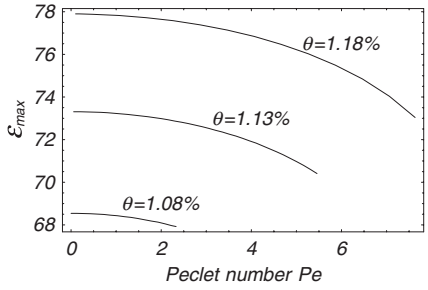

Figure 2. Maximum scalar conductivity enhancements versus normalized shear rate for steady logrolling orientational states at volume fractions of 1.08, 1.13, and 1.18% for nanorods of aspect ratio 200.

Figure 3 shows the dynamic property fluctuations of tumbling (T) and wagging (W) stable sheared responses at volume fraction $\theta_2 = 1.08$ % ($N = 5.5$). The maximum scalar conductivity, σ^e_{max}, is on the order of 35–75 times the matrix conductivity, σ_1; recall the conductivity contrast is $\sigma_2/\sigma_1 = 10^6$. The horizontal axis shows the large dynamic range of the maximum effective conductivity,

$$\frac{\max\varepsilon_1(t)}{\min\varepsilon_1(t)} \approx \begin{cases} 1.5 & \text{for W orbits,} \\ 2 & \text{for T orbits;} \end{cases} \tag{14}$$

the vertical axis, $\varepsilon_1(t) - \varepsilon_2(t)$, shows the high degree and large dynamic range of anisotropy,

$$\frac{\max(\varepsilon_1(t) - \varepsilon_2(t))}{\min(\varepsilon_1(t) - \varepsilon_2(t))} \approx \begin{cases} 4 & \text{for W orbits,} \\ 8 & \text{for T orbits.} \end{cases} \tag{15}$$

The tumbling attractor transitions to wagging as the shear rate increases at these volume fractions.

Figure 4 shows the corresponding results for the oscillatory kayaking state (K_1) whose peak orientation rotates about the vorticity axis with volume fraction $\theta_2 = 1.02$ % ($N = 5.2$) and shear rate $Pe = 3$. The maximum scalar conductivity, σ^e_{max}, is on

ADVANCED FUNCTIONAL MATERIALS

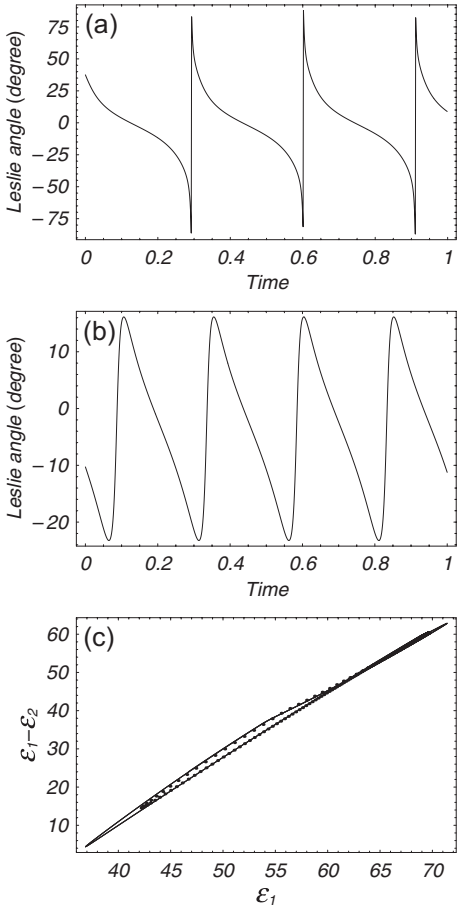

Figure 3. Dynamic ranges at volume fraction 1.08 % of nanorods with an aspect ratio of 200: the peak-alignment direction for tumbling (a, $Pe = 3.4$) and wagging (b, $Pe = 4$) sheared monodomains; and (c) corresponding maximum scalar effective conductivity enhancement $\varepsilon_1 = \varepsilon_{max}$ and effective conductivity anisotropy measure $\varepsilon_1 - \varepsilon_2$, where tumbling values are solid and wagging values are dotted.

the order of 60 ± 2 times the matrix conductivity, σ_1. The horizontal axis shows a smaller dynamic range of ε_1 than tumbling or wagging phases, with:

$$\frac{\max \varepsilon_1(t)}{\min \varepsilon_1(t)} \approx 1.05. \tag{16}$$

The vertical axis, $\varepsilon_1 - \varepsilon_2$, shows large anisotropy of the effective conductivity, $\mathbf{\Sigma}^e$, with a relatively small dynamic range:

$$\frac{\max(\varepsilon_1(t) - \varepsilon_2(t))}{\min(\varepsilon_1(t) - \varepsilon_2(t))} \approx 1.1. \tag{17}$$

Figure 5 shows corresponding results for the tilted kayaking limit cycle (K_2) at slightly higher volume fraction $\theta_2 = 1.08$ % and $Pe = 6$. In this case, the maximum scalar conductivity is

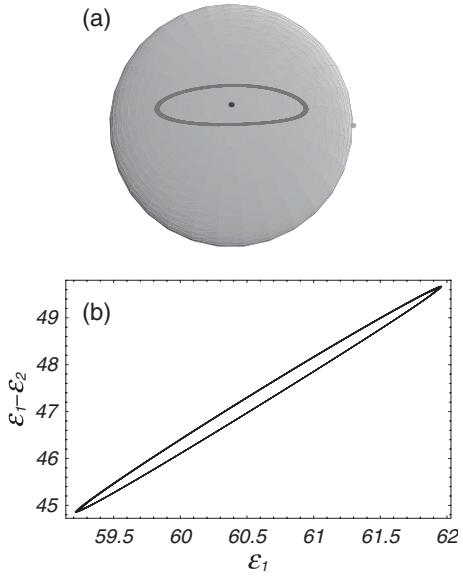

Figure 4. a) Dynamics of the peak orientation of the PDF around the vorticity axis (the dot in the middle), and b) the dynamic ranges of ε_1 and $\varepsilon_1 - \varepsilon_2$, for a typical kayaking limit cycle (K_1) at normalized shear rate $Pe = 3$, nanorod volume fraction 1.02 %, and nanorod aspect ratio 200.

again on the order of 60 ± 5 times the matrix conductivity σ_1. The horizontal axis shows a larger dynamic range of ε_1 compared to the K_1 state of Figure 4,

$$\frac{\max \varepsilon_1(t)}{\min \varepsilon_1(t)} \approx 1.16, \tag{18}$$

and the vertical axis of $\varepsilon - \varepsilon_2$ shows less, but still significant, anisotropy of the effective conductivity, $\mathbf{\Sigma}^e$, and large dynamic range,

$$\frac{\max(\varepsilon_1(t) - \varepsilon_2(t))}{\min(\varepsilon_1(t) - \varepsilon_2(t))} \approx 1.5. \tag{19}$$

The analogous results for chaotic orientational sheared responses is shown in Figure 6, with volume fraction $\theta_2 = 1.02$ % ($N = 5.2$) and $Pe = 4.044$. The maximum scalar conductivity is on the order 35–65 times the matrix conductivity, σ_1. The horizontal axis shows the largest dynamic range of ε_1 for all states,

$$\frac{\max \varepsilon_1(t)}{\min \varepsilon_1(t)} \approx 1.85, \tag{20}$$

and the vertical axis of $\varepsilon_1 - \varepsilon_2$ shows large anisotropy of the effective conductivity with large dynamic fluctuations,

$$\frac{\max(\varepsilon_1(t) - \varepsilon_2(t))}{\min(\varepsilon_1(t) - \varepsilon_2(t))} \approx 26.0. \tag{21}$$

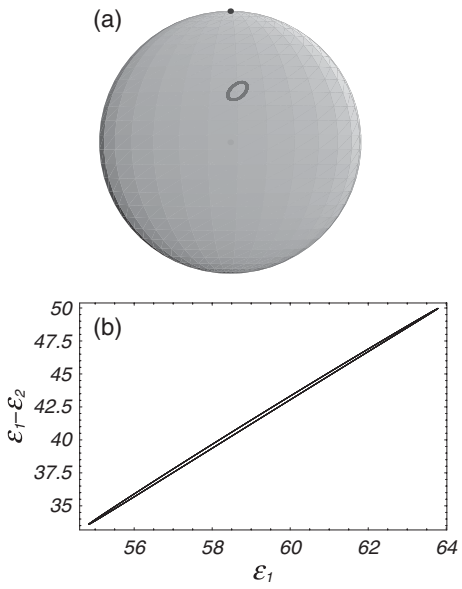

Figure 5. a) Dynamics of the peak orientation axis of the PDF around the vorticity axis (the dot in the middle), and b) the dynamic ranges of ε_1 and $\varepsilon_1-\varepsilon_2$ for a typical tilted kayaking state (K_2) at higher shear rate, $Pe=6$, nanorod volume fraction 1.08 %, and nanorod aspect ratio 200.

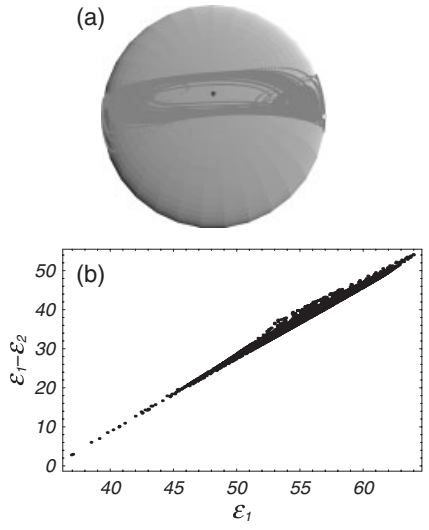

Figure 6. a) Chaotic orbit of the peak orientation axis of the nanocomposite PDF at moderate shear rate $Pe=4.044$, nanorod volume fraction 1.02 %, and aspect ratio 200. b) The dynamic ranges of ε_1 and $\varepsilon_1-\varepsilon_2$ for this chaotic monodomain.

Finally, we give the effective property analog of a bifurcation diagram (Fig. 7) in time-averaged, maximum enhancement (ε_{max}) of the effective conductivity tensor, $\mathbf{\Sigma}^e$, versus normalized shear rate, *Pe*, for fixed normalized concentration, $N=5.2$, corresponding to volume fraction $\theta_2=1.02$ %. These bifurcation diagrams are now standard in the rheology literature on sheared nematic polymer monodomains, where, typically, the vertical axis is the amplitude of projection of the PDF onto one spherical harmonic. The diagrams show the effective property

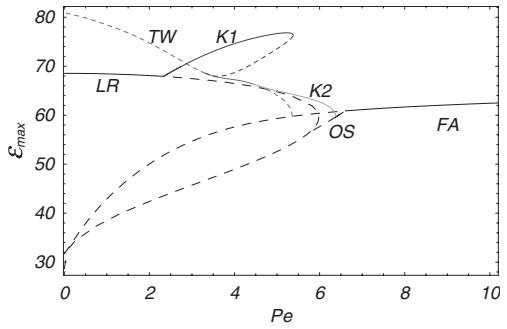

Figure 7. "Property bifurcation diagram" of maximum conductivity enhancement vs. normalized shear rate for nanorod composites of nanorod volume fraction 1.02 % and aspect ratio 200. Solid (dashed) curves indicate stable (unstable) sheared nanocomposite monodomains. LR, OS, FA denote distinct steady states; TW, K_1, K_2 denote distinct limit cycles, for which time-averaged values of ε_{max} are given.

transitions versus shear rate between the various stable (solid curves) and unstable (dashed curves) sheared response modes of the NPNC. For this specific volume fraction, this "property bifurcation diagram" shows that the kayaking state (K_1) attains the maximum enhancement. The diagram also shows the maximum effective conductivity increases with shear rate for stable K_1 and FA states, yet it decreases for LR, T, W, and K_2 states. Furthermore, when the K_1 branch is lost at the indicated *Pe*, the new stable state (K_2) acquires a discontinuous drop in ε_{max}! This result, in nonlinear-physics parlance on sheared nematic polymer liquids, is a first-order phase transition, a shear-induced analog of the isotropic–nematic phase transition. The message here is that property tensors inherit these phase transitions! Furthermore, there are processing windows of *Pe* with bistable and even tristable monodomain responses. In the paper by Zheng et al.,[25] likelihood and expected-time statistics are developed that address the role of initial conditions and basins of attraction for multiple attractors. For example, in the region where K_1 and W are bistable, the attracting set of K_1 is three times larger than that of W if the initial data is random. However, initial prealignment of monodomains by mechanical rubbing or chemical plate treatment can strongly bias the distribution in favor of in-plane W or out-of-plane K_1 attractors.

5. Conclusion

Sheared monodomains of high-aspect-ratio nematic polymers in viscous solvents are modeled by Doi–Hess kinetic theory, which yields the orientational probability distribution function versus volume fraction and shear rate. Numerical databases for these distribution functions[1,2] are implemented here in homogenization formulas[3] for the effective conductivity tensor $\mathbf{\Sigma}^e$, requiring information on the volume fractions, θ_1, θ_2, and scalar conductivities, σ_1, σ_2, of the matrix solvent and nematic polymer nanophase, respectively. We have illustrated typical gains and dynamic fluctuations in both maximum conductivity and conductive anisotropy for steady and unsteady sheared monodomain distribution functions. From these pre-

ADVANCED FUNCTIONAL MATERIALS

dictions, we also give relative comparisons among the variety of processing-induced monodomain distributions. These results suggest that there is a clear potential in using tools such as these to optimize or control property gains in NPNCs. The next step in this program is to allow for heterogeneity, where the results of this paper are extended to a spatially varying ensemble of local monodomain attractors.[21]

Received: May 2, 2005
Final version: July 25, 2005

[1] M. G. Forest, Q. Wang, R. Zhou, *Rheol. Acta* **2004**, *43*, 17.
[2] M. G. Forest, Q. Wang, R. Zhou, *Rheol. Acta* **2004**, *44*, 80.
[3] X. Zheng, M. G. Forest, R. Lipton, R. Zhou, Q. Wang, *Adv. Funct. Mater.* **2005**, *15*, 627.
[4] M. Kroger, *Phys. Rep.* **2004**, *390*, 453.
[5] S. Hess, M. Kroger, *J. Phys.: Condens. Matter* **2004**, *16*, s3835.
[6] G. Rienacker, S. Hess, *Physica A* **1999**, *267*, 294.
[7] G. Rienacker, M. Kroger, S. Hess, *Phys. Rev. E* **2002**, *66*, 040 702.
[8] V. Faraoni, M. Grosso, S. Crescitelli, P. L. Maffettone, *J. Rheol.* **1999**, *43*, 829.
[9] M. G. Forest, Q. Wang, *Rheol. Acta* **2003**, *42*, 20.
[10] M. G. Forest, Q. Wang, R. Zhou, E. Choate, *J. Non-Newtonian Fluid Mech.* **2004**, *118*, 17.
[11] M. G. Forest, R. Zhou, Q. Wang, *Phys. Rev. Lett.* **2004**, *93*, 088 301.
[12] M. G. Forest, Q. Wang, H. Zhou, R. Zhou, *J. Rheol.* **2004**, *48*, 175.
[13] M. G. Forest, R. Zhou, Q. Wang, *Multiscale Model. Simul.*, in press.
[14] H. Zhou, M. G. Forest, X. Zheng, Q. Wang, R. Lipton, *Macromol. Symp.* **2005**, *28*, 81.
[15] R. Zhou, M. G. Forest, Q. Wang, *Multiscale Model. Simul.* **2004**, *3*, 853.
[16] M. G. Forest, R. Zhou, Q. Wang, *J. Rheol.* **2003**, *47*, 105.
[17] R. Bandyopadhyay, G. Basappa, A. K. Sood, *Phys. Rev. Lett.* **2000**, *84*, 2022.
[18] B. Chakrabarti, M. Das, C. Dasgupta, S. Ramaswamy, A. K. Sood, *Phys. Rev. Lett.* **2004**, *92*, 055 501.
[19] A. D. Rey, M. M. Denn, *Annu. Rev. Fluid Mech.* **2002**, *34*, 233.
[20] G. Sgalari, G. L. Leal, J. J. Feng, *J. Non-Newtonian Fluid Mech.* **2002**, *102*, 361.
[21] M. G. Forest, R. Zhou, Q. Wang, X. Zheng, R. Lipton, in *Proc. of Workshop on "Modeling of Soft Matter"* (Eds.: M.-C. T. Calderer, E. M. Terentjev), Springer, New York **2005**, Vol. 141, p. 85.
[22] M. Doi, *J. Polym. Sci., Polym. Phys. Ed.* **1981**, *19*, 229.
[23] S. Hess, *Z. Naturforsch. A* **1976**, *31A*, 1034.
[24] M. Grosso, R. Keunings, S. Crescitelli, P. L. Maffettone, *Phys. Rev. Lett.* **2001**, *86*, 3184.
[25] X. Zheng, M. G. Forest, R. Zhou, Q. Wang, *Rheol. Acta* **2005**, *44*, 219.

